Contribution from the Istituto di Chimica Farmaceutica, Università di Milano, I-20131 Milano, Italy, Spectrospin AG, CH-8117 Fällanden, Switzerland, Laboratorium für anorganische Chemie, ETH-Z, CH-8092 Zürich, Switzerland, and Laboratoire de Chimie de Coordination, UA 416 du CNRS, Université Louis Pasteur, F-67070 Strasbourg Cédex, France

Gold and Silver Hydrides: Synthesis of Heterobimetallic Ir-M (M = Au, Ag) Complexes and X-ray Crystal Structures of $[(PPh_3)Au(\mu\text{-}H)IrH_2(PPh_3)_3](BF_4)$ and $[(PPh_3)Ag(\mu\text{-}H)IrH_2(PPh_3)_3](CF_3SO_3)$

Alberto Albinati,[1a] Clemens Anklin,[1b] Philipp Janser,[1c] Hans Lehner,[1c] Dominique Matt,[1d] Paul S. Pregosin,[1c] and Luigi M. Venanzi*[,1c]

Received August 22, 1988

The hydrido-bridged cationic complexes $[(PR_3)M(\mu\text{-}H)IrH_2(PPh_3)_3](CF_3SO_3)$ (M = Au, Ag; R = Ph, Et) have been prepared and characterized by NMR (^1H, ^{31}P, and ^{109}Ag) and crystallographic methods. The three PPh_3 ligands on iridium have *mer* geometry. The complexes show dynamic behavior in solution, which exchanges the bridging hydride with the terminal hydride trans to PPh_3. It is shown that the $J(^{109}Ag,^1H)$ values obtained from the two-dimensional ^{109}Ag NMR spectra are useful in distinguishing bridging from terminal hydrides. The crystals of $[(PPh_3)Au(\mu\text{-}H)IrH_2(PPh_3)_3](BF_4)\cdot CH_2Cl_2$ (**1b**·CH_2Cl_2) belong to space group $P\bar{1}$ with $Z = 2$, $a = 17.482$ (6) Å, $b = 15.617$ (5) Å, $c = 13.218$ (5) Å, $\alpha = 90.97$ (4)°, $\beta = 71.38$ (3)°, $\gamma = 103.89$ (5)°, and $V = 3312.9$ (4) Å^3. The structure was refined by block-diagonal least squares to $R = 0.054$ for the 3792 observed reflections. The crystals of $[(PPh_3)Ag(\mu\text{-}H)IrH_2(PPh_3)_3](CF_3SO_3)$ (**3**), in the form of its benzene solvate, belong to the monoclinic space group Cc with $Z = 4$, $a = 19.461$ (4) Å, $b = 19.458$ (5) Å, $c = 20.054$ (4) Å, $\beta = 96.16$ (2)°, and $V = 7550.3$ (4) Å^3. The structure was refined by full-matrix least squares to $R = 0.049$ for the 2842 observed reflections.

Introduction

It is now well established that many transition-metal hydrides are capable of combining with electron-deficient species to afford bimetallic complexes containing $M(\mu\text{-}H)M'$ linkages.[2,3] The stabilization thus obtained allows in particular the formation of hydrido complexes with metals such as gold and silver, for which mononuclear hydrides are either unknown or very unstable.[4-6]

The current interest in polynuclear hydrido-gold complexes is mainly due to their unusual structural features and their potential use as catalyst precursors.[7,8] Furthermore, additional information on gold-hydride interactions could be relevant to gold alloy surface catalysis.[9] Metal-hydrogen-gold interactions have already been directly observed in some complexes, e.g., $[\{(PPh_3)Au(\mu\text{-}H)\}_2Ru(dppm)_2](NO_3)$[6c] (dppm = $Ph_2PCH_2PPh_2$) and $[(PPh_3)Au(\mu\text{-}H)Pt(C_6F_5)(PEt_3)_2](CF_3SO_3)$.[10]

In a preliminary communication we described the cations $[(L)Au(\mu\text{-}H)IrH_2(PPh_3)_3]^+$ (L = PPh_3, PEt_3).[5] We report here their syntheses and that of their silver analogues, together with the X-ray crystal structures of $[(PPh_3)Au(\mu\text{-}H)IrH_2(PPh_3)_3](BF_4)$ (**1b**) and $[(PPh_3)Ag(\mu\text{-}H)IrH_2(PPh_3)_3](CF_3SO_3)$ (**3**).

Results and Discussion

a. Gold Complexes. The bimetallic gold-iridium complexes **1a** and **2** were prepared in high yield according to eq 1. Complexes **1a** and **2** were characterized in solution by ^1H and $^{31}P\{^1H\}$ NMR spectroscopy. Their low-temperature ^{31}P NMR spectra are consistent with the solid-state structure. They show three sets of sharp signals, which can be assigned to P^1, $P^{2,3}$, and P^4 (see Table I). The most significant feature is the observation of a coupling between P^1 and P^4, 19 and 16 Hz for **1a** and **2**, respectively, which confirms the postulation of bimetallic species in solution. This coupling is the combination of $^3J(P^1,P^4)$ via the Au-Ir bond and of $^4J(P^1,P^4)$ via the μ-H bridge. The corresponding room-temperature spectra are broad, indicating that dynamic processes are occurring in solution at that temperature. More information about this process is provided by their ^1H NMR spectra. The hydride region of the ^1H NMR spectrum (CD_2Cl_2, 233 K) of **1a** shows three sets of signals, which can be assigned to H^1 ($\delta = -4.49$), H^2 ($\delta = -9.24$), and H^3 ($\delta = -11.18$) (see Table I). Assignment of the individual resonances could be unambiguously made by selective $^1H\{^{31}P\}$ experiments. These show that H^1 is simultaneously coupled to P^1 and P^4 ($^2J(P^1,H^1) = 79$ Hz and $^2J(P^4,H^1) = 12$ Hz, respectively). It is interesting to note that the H^1 and H^2 hydride signals are low-field-shifted relative to those of the starting complex *mer*-$IrH_3(PPh_3)_3$ (δ_H(trans H) = -10.91 and δ_H(trans P) = -12.68). However, while the chemical shifts of the terminal hydride ligands H^2 and H^3 show only moderate changes relative to those in the parent compound, that of the hydride attached to gold, H^1, is significantly shifted downfield in agreement with what has been observed in related hydrido-bridged systems.[11] It should also be noted that, as found in other complexes containing the fragment H-Ir-H-M,[11c] the

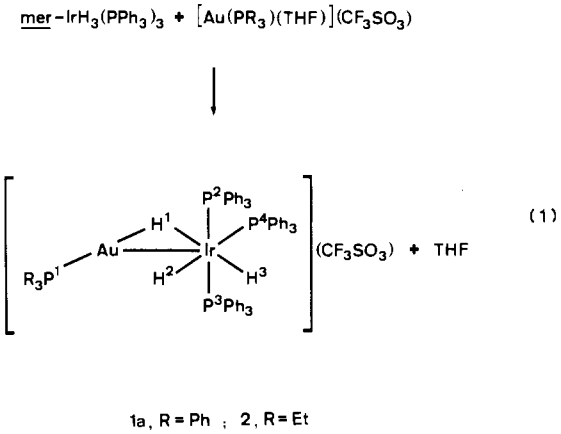

1a, R = Ph ; 2, R = Et

(1) (a) Università di Milano. (b) Spectrospin AG. (c) ETH Zürich. (d) Université Louis Pasteur.
(2) Venanzi, L. M. *Coord. Chem. Rev.* **1982**, *43*, 251.
(3) Hlatki, G. G.; Johnson, B. F. G.; Lewis, J.; Raithby, P. R. *J. Chem. Soc., Dalton Trans.* **1985**, 1277 and references quoted therein.
(4) Green, M.; Orpen, A. G.; Salter, I. D.; Stone, F. G. A. *J. Chem. Soc., Dalton Trans.* **1984**, 2497.
(5) Lehner, H.; Matt, D.; Pregosin, P. S.; Venanzi, L. M.; Albinati, A. *J. Am. Chem. Soc.* **1982**, *104*, 6825.
(6) (a) Casalnuovo, A. L.; Pignolet, L. H.; van der Velden, J. W. A.; Bour, J. J.; Steggerda, J. J. *J. Am. Chem. Soc.* **1983**, *105*, 5957. (b) Boyle, P. D.; Johnson, B. J.; Buehler, A.; Pignolet, L. H. *Inorg. Chem.* **1986**, *25*, 7. (c) Alexander, B. D.; Johnson, B. J.; Johnson, S. M.; Casalnuovo, A. L.; Pignolet, L. H. *J. Am. Chem. Soc.* **1986**, *108*, 4409. (d) Casalnuovo, A. L.; Laska, T.; Nilsson, P. V.; Olofson, J.; Pignolet, L. H.; Bos, W.; Bour, J. J.; Steggerda, J. J. *Inorg. Chem.* **1985**, *24*, 182. (e) Boyle, P. D.; Johnson, B. J.; Alexander, B. D.; Casalnuovo, J. A.; Gannon, P. R.; Johnson, S. M.; Larka, E. A.; Mueting, A. M.; Pignolet, L. H. *Inorg. Chem.* **1987**, *26*, 1346. (f) Alexander, B. D.; Boyle, P. D.; Johnson, B. J.; Casalnuovo, J. A.; Johnson, S. M.; Mueting, A. M.; Pignolet, L. H. *Inorg. Chem.*, in press. (g) Alexander, B. D.; Johnson, B. J.; Johnson, S. M.; Boyle, P. D.; Kann, N. C.; Mueting, A. M.; Pignolet, L. H. *Inorg. Chem.* **1987**, *26*, 3506.
(7) Schwank, J. *Gold Bull.* **1985**, *18*, 1.
(8) Braunstein, P.; Rosé, J. *Gold Bull.* **1988**, *18*, 17.
(9) Sinfelt, J. H. *Bimetallic Catalysis*; Wiley: New York, 1983; Chapter 2.
(10) Albinati, A.; Lehner, H.; Venanzi, L. M.; Wolfer, M. *Inorg. Chem.* **1987**, *26*, 3933.
(11) (a) Braunstein, P.; Gomes Carneiro, T. M.; Matt, D.; Tiripicchio, A.; Tiripicchio Camellini, M. *Angew. Chem., Int. Ed. Engl.* **1986**, *25*, 748. (b) McGilligan, B. S.; Venanzi, L. M.; Wolfer, M. *Organometallics* **1987**, *5*, 947. (c) Boron, P.; Musco, A.; Venanzi, L. M. *Inorg. Chem.* **1982**, *21*, 4192.

0020-1669/89/1328-1105$01.50/0

Table I. Selected NMR Data for Complexes **1–4**[a]

cation	δ (J, Hz) ^{1}H	^{31}P{^{1}H}
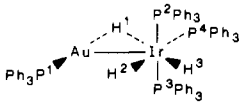 **1a**[b]	−4.49 (H^1, $^2J(P^1,H^1)$ = 79.3, $^2J(P^4,H^1)$ = 12.4) −9.24 (H^2, $^2J(P^4,H^2)$ = 101.3, $^2J(P^{2,3},H^2)$ = 18.3, $J(P^1,H^2)$ = 15.9) −11.18 (H^3, $J(P^1,H^3)$ = 17.3, $^2J(P^{2,3},H^3)$ = 19.2, $^2J(P^4,H^2)$ = 10.3)	48.2 (P^1, $J(P^1,P^4)$ = 19) 13.9 (P^4, $J(P^4,P^1)$ = 19, $^2J(P^4,P^{2,3})$ = 17) 2.8 ($P^{2,3}$, $^2J(P^{2,3},P^4)$ = 17)
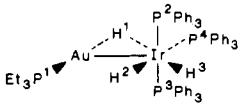 **2**[c]	−4.39 (H^1, $^2J(P^1,H^1)$ = 75.7, $^2J(P^4,H^1)$ = 13) −9.43 (H^2, $^2J(P^4,H^2)$ = 101.3, $^2J(P^{2,3},H^2)$ = 19.5, $J(P^1,H^2)$ = 13.4) −11.29 (H^3, $J(P^1,H^3)$ = 17, $^2J(P^2,H^3)$ = 17, $^2J(P^4,H^3)$ = ca. 10)	47.3 (P^1, $J(P^1,P^4)$ = 16) 14.4 (P^4, $J(P^4,P^1)$ = 16, $^2J(P^4,P^{2,3})$ = 15) 3.3 ($P^{2,3}$, $^2J(P^{2,3},P^4)$ = 15)
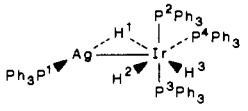 **3**[d]	−8.56 (H^1, $^2J(P^1,H^1)$ = 33, $^2J(P^4,H^1)$ = 7, $^2J(P^2,H^1)$ = 6, $^2J(H^1,H^3)$ = 6, $J(^{109}Ag,H^1)$ = 116) −11.09 (H^3, $J(^{109}Ag,H^3)$ = 15) −11.54 (H^2, $^2J(P^4,H^2)$ = 97, $J(^{109}Ag,H^2)$ = 23)	17.8 (P^1, $J(P^1,P^4)$ = 15, $^1J(^{107}Ag,P^1)$ = 537, $^1J(^{109}Ag,P^1)$ = 617) 10.3 (P^4, $J(P^4,P^1)$ = 15, $^2J(P^4,P^{2,3})$ = 18, $J(^{109}Ag,P^4)$ = 36) 5.2 ($P^{2,3}$, $^2J(P^{2,3},P^4)$ = 18)
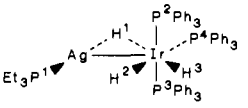 **4**[e]	−8.72 (H^1, $^2J(P^1,H^1)$ = 31, $J(^{109}Ag,H^1)$ = 102) −11.19 (H^3, $J(^{109}Ag,H^3)$ = ca. 12) −11.64 (H^2, $^2J(P^4,H^2)$ = 76, $J(^{109}Ag,H^2)$ = 24)	14.0 (P^1, $J(P^1,P^4)$ = 13, $^1J(^{107}Ag,P^1)$ = 524, $^1J(^{109}Ag,P^1)$ = 508) 11.2 (P^4, $J(P^4,P^1)$ = 13, $^2J(P^4,P^{2,3})$ = 17) 5.4 ($P^{2,3}$, $^2J(P^{2,3},P^4)$ = 17)

[a] Coupling constant indices have been omitted where the number of bonds between the coupled nuclei can take more than one value. [b] All spectra recorded in CD_2Cl_2 (^{1}H) or CH_2Cl_2–CD_2Cl_2 (^{31}P). 233 K for **1a**. [c] 173 K. [d] 253 K; $\delta_{^{109}Ag}$ = −1261 (relative to $AgNO_3$), nine-line multiplet with line separation of ca. 10 Hz. [e] 253 K, $\delta_{^{109}Ag}$ = −1056 (relative to $AgNO_3$).

values of the $^2J(H,H)_{trans}$ coupling constants are less than 6 Hz.

The room-temperature spectrum of **1a** also shows three sets of signals in the hydride region; however, while those due to H^3 are sharp, the others are broad, indicating that a dynamic process is occurring at this temperature. This was confirmed by selective irradiation experiments; e.g., saturation of the resonances due to H^1 transfers the saturation to those due to H^2 (see Figure 1). As the signals due to H^3 remain sharp, either when the temperature is raised or when the H^1 signals are saturated, a migration of the "$Au(PPh_3)$" fragment from H^1 to H^3 can be excluded. In this context it should be noted that irradiation of the resonance due to H(trans H) in *mer*-$IrH_3(PPh_3)_3$ results in the complete disappearance of the signal due to H(trans P).[12]

It is worth noting that *mer*- and *fac*-$IrH_3(PMe_2Ph)_3$ can be protonated to give a single product, formulated as $[IrH_2(H_2)(PMe_2Ph)_3]^+$.[13] Given the isolobal analogy between H^+ and $[(AuR_3P)]^+$,[14] the dynamics for compounds **1a** and **2** might then be viewed as arising as shown in Scheme I. However, we have discarded both of these possibilities since (a) the first of them requires an equilibrium between as yet undetected isomers (we thank a reviewer for calling this to our attention) and (b) the T_1 values for H^1, H^2, and H^3 (0.26, 0.30, and 0.18 s, respectively) are not consistent with the formation of short H^1–H^2 contacts.[15]

Finally, we wish to emphasize that acetone or dichloromethane solutions of complexes **1a** and **2** are stable at room temperature in contrast with other bimetallic hydrido-bridged Ir–Au cations, such as $[(PPh_3)Au(\mu\text{-}H)_2Ir(acetone)_2(PPh_3)_2]^{2+}$ or $[(PPh_3)Au(\mu\text{-}H)IrH(NO_3)(PPh_3)_2]^+$.[6d]

X-ray Crystal Structure of $[(PPh_3)Au(\mu\text{-}H)IrH_2(PPh_3)_3](BF_4)\cdot CH_2Cl_2$ (1b·CH_2Cl_2). The structure of this compound consists of discrete cations, BF_4^- anions, and clathrated CH_2Cl_2. An ORTEP view of the metal and donor atoms in the cation is shown in Figure 2. An ORTEP view of the cation has appeared elsewhere.[5] A list of relevant bond lengths and angles is given in Table II.

The cation consists of an octahedrally coordinated iridium atom joined to a gold atom through a single Au–H–Ir bridge. The value of the torsion angle P^1–Au–Ir–P^4 (175°) indicates that the complex

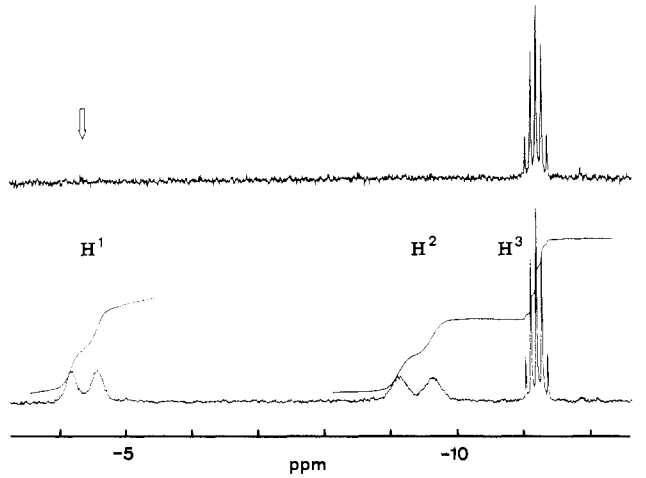

Figure 1. Room-temperature ^{1}H NMR spectra (hydride region) of **1a**: (a) normal spectrum; (b) spectrum with irradiation at H^1.

Scheme I

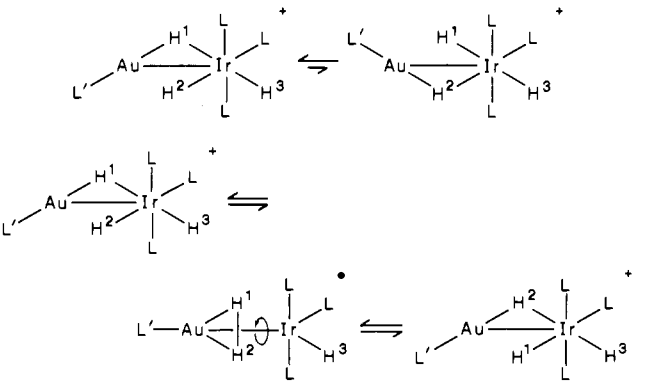

can be visualized as having an approximate plane of symmetry going through these four atoms as well as H^1, H^2, and H^3.

The value of the Au–Ir distance (2.765 (1) Å) is comparable with (1) the Cr–Au distance (2.770 (2) Å) in $(PPh_3)Au(\mu\text{-}H)Cr(CO)_5$,[4] (2) the average Ru–Au distances (2.781 (7) Å) in $[\{(PPh_3)Au(\mu\text{-}H)\}_2Ru(dppm)_2](NO_3)$,[6c] and (3) the Au–Pt dis-

(12) Whitmore, B. C.; Eisenberg, R. *Inorg. Chem.* **1984**, *23*, 1697.
(13) Lundquist, E. G.; Huffman, J. C.; Folting, K.; Caulton, K. G. *Angew. Chem., Int. Ed. Engl.*, in press.
(14) Evans, D. G.; Mingos, D. M. P. *J. Organomet. Chem.* **1982**, *232*, 171.
(15) Crabtree, R. H.; Hamilton, D. G. *Adv. Organomet. Chem.* **1988**, *28*, 299.

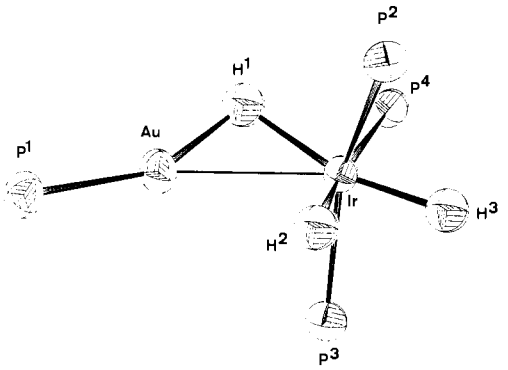

Figure 2. ORTEP view of the metal and donor atoms in the $[(PPh_3)Au(\mu\text{-}H)IrH_2(PPh_3)_3]^+$ cation.

Table II. Bond Distances (Å) and Bond Angles and Torsion Angles (deg) for the Complexes $[(PPh_3)Au(\mu\text{-}H)IrH_2(PPh_3)_3](BF_4)\cdot CH_2Cl_2$ (**1b**·CH_2Cl_2) and $[(PPh_3)Ag(\mu\text{-}H)IrH_2(PPh_3)_3](CF_3SO_3)\cdot 2C_6H_6$ (**3**·$2C_6H_6$)

	1b, M = Au	**3**, M = Ag
Ir–M	2.765 (1)	2.758 (2)
M–P^1	2.265 (5)	2.384 (6)
Ir–P^2	2.334 (6)	2.328 (5)
Ir–P^3	2.325 (6)	2.291 (5)
Ir–P^4	2.397 (4)	2.362 (5)
Ir–H^1	1.90[a]	1.4 (2)
Ir–H^2	1.72[a]	1.7 (1)
Ir–H^3	1.71[a]	1.8 (2)
M–H^1	1.87[a]	1.8 (2)
P^1–M–Ir	155.3 (3)	160.1 (2)
M–Ir–P^2	100.3 (1)	90.3 (1)
M–Ir–P^3	87.4 (1)	89.0 (1)
M–Ir–P^4	115.6 (1)	126.6 (1)
P^2–Ir–P^3	149.9 (2)	153.2 (2)
P^2–Ir–P^4	100.2 (2)	100.6 (2)
P^3–Ir–P^4	102.7 (2)	101.2 (2)
M–H–Ir	94[a]	118 (8)
P^2–Ir–H^1	93[a]	91 (8)
P^3–Ir–H^1	112[a]	104 (8)
P^4–Ir–H^1	76[a]	91 (8)
P^4–Ir–H^3	173[a]	172 (4)
H^1–Ir–H^2	163[a]	172 (9)
H^2–Ir–H^3	83[a]	81 (9)
P^1–M–Ir–P^4	174.7 (5)	176.7 (6)
P^1–M–Ir–P^2	68.2 (5)	−73.2 (6)

[a] Calculated values (see the Experimental Section).

tance of 2.714 (1) Å in $[(PPh_3)Au(\mu\text{-}H)Pt(C_6F_5)(PEt_3)_2](CF_3SO_3)$.[10] Although these distances are slightly longer than the Au–M distances where there is only a direct Au–M bond, e.g., 2.625 (1) Å in $[(Ph_3P)AuIr(dppm)_2](BF_4)_2$,[16] they still indicate a significant Au–M interaction. This view is supported by structural data for related complexes that do not contain gold. Thus (1) the Cr–Cr distance in $[K(crypt\text{-}222)][(CO)_5Cr(\mu\text{-}H)Cr(CO)_5]$ is 3.300 (4) Å,[17] (2) the Rh–Ru distance in $(C_8H_{12})Rh(\mu\text{-}H)\{\mu\text{-}(C_6H_5)PCH_2P(C_6H_5)_2\}Ru(Ph)(dppm)$ is 2.941 (1) Å,[18] and (3) the Pt–Pt distance in $[(PEt_3)_2PhPt(\mu\text{-}H)PtPh(PEt_3)_2](BPh_4)$ is 3.238 (1) Å.[19]

It should be noted that the Au–Ir distance in **1b** (2.765 (1) Å), where the structural data indicate the formation of a single Au–H–Ir bridge, is significantly longer than the Au–Ru distance (2.694 (1) Å) in $[(PPh_3)Au(\mu\text{-}H)_2Ru(dppm)_2](PF_6)$, in which a double Au–H–Ru bridge is present.[6g]

The hydride ligands could not be positioned on the basis of the X-ray data, and therefore, their localization was attempted by using the program HYDEX. This gave three energy minima in agreement with the expected positions of the hydride ligands. The calculated Au–H–Ir angle (94°), although very small, is comparable, within the limits of the method, with other Au–H–M angles in compounds where the H atoms were refined; e.g., Au–H–Cr is 111 (5)° in $(Ph_3P)Au(\mu\text{-}H)Cr(CO)_5$[4] and Au–H–Pt is 103 (4)° in $[(PPh_3)Au(\mu\text{-}H)Pt(C_6F_5)(PEt_3)_2](CF_3SO_3)$.[10] These angles are much smaller than those found in compounds with long M–M distances; e.g., Cr–H–Cr is 145.1 (3)° in the compound mentioned earlier.[17]

A distorted-digonal coordination at the gold atom can be deduced from the observed heavy atoms and the calculated hydrogen positions, which give the following distances and angles: Au–H^1 = 1.87 Å, Au–H^2 = 2.76 Å, P^1–Au–Ir = 155.3 (3)°, and P^1–Au–H^1 = 156°. The distorted-octahedral geometry around the iridium atom has been discussed elsewhere[5,20] and will not be commented upon here, except for the mention of the long Ir–P^4 distance, which is indicative of the strong trans influence of the terminal hydride H^2. This point will be discussed more fully in connection with the analogous silver complex.

b. Silver Complexes. For the preparation of the related silver complexes **3** and **4**, 1:1 mixtures of $AgCF_3SO_3$ and the corresponding phosphine were reacted with *mer*-$IrH_3(PPh_3)_3$ (see the Experimental Section). These reactions are quantitative. The

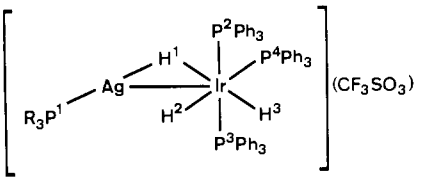

3, R = Ph ; **4**, R = Et

proposed structures are based on microanalytical and ^1H and ^{31}P NMR data. The $^{31}P\{^1H\}$ NMR spectrum of **3** measured at 253 K displays three sets of signals at 17.8 (P^1), 10.3 (P^4), and 5.2 ppm ($P^{2,3}$), respectively (see Table I). The signals due to P^1 appear as two doublets of doublets (intensity ca. 1:1) due to coupling with ^{107}Ag and ^{109}Ag ($J(^{107}Ag,P^1)$ = 537 Hz, $J(^{109}Ag,P^1)$ = 617 Hz). The binuclear nature of complexes **3** and **4** is established by the existence of a $J(P^1,P^4)$ coupling constant of 15 Hz. In the room-temperature $^{31}P\{^1H\}$ NMR spectrum, the signals due to P^1 and P^4 are broader than those due to P^2 and P^3. However, the former set sharpens at low temperatures while those of $P^{2,3}$ remain practically unchanged. This suggests a dynamic behavior similar to that of **1** or **2** for this molecule, i.e., involving basically a motion localized in the plane of symmetry of this complex.

As in **1a** and **2**, the hydride ligands in **3** appear as three sets of signals in its ^1H NMR spectrum (Table I).

A first-order analysis of the ^1H NMR spectrum for **3** proved possible with the help of an inverse ^1H, ^{109}Ag two-dimensional spectrum[21] (see Figure 3). In this methodology only the signals coupled to the ^{109}Ag spin appear, thereby simplifying the spectrum. The multiplicities of the signals in the rows arise from silver–proton couplings, whereas those in the columns (silver-109 resonance) arise from phosphorus atoms of the proton-decoupled metal spectrum.

All three hydrides couple to silver, but with very different values. The 116-Hz value for the low-field bridging hydride, H^1, is consistent with a one-bond interaction[22] and in our experience[23] is on the high side of the 81–122-Hz range. Of equal interest are

(16) Casalnuovo, A. L.; Laska, T.; Nilsson, P. V.; Olofson, J.; Pignolet, L. H. *Inorg. Chem.* **1985**, *24*, 233.
(17) Peterson, J. L.; Brown, R. K.; Williams, J. M. *Inorg. Chem.* **1981**, *20*, 158.
(18) Delavaux, B.; Chaudret, B.; Dahan, F.; Poilblanc, R. *Organometallics* **1985**, *4*, 935.
(19) Carmona, D.; Thouvenot, R.; Venanzi, L. M.; Bachechi, F.; Zambonelli, L. *J. Organomet. Chem.* **1983**, *250*, 589.
(20) Albinati, A.; Lehner, H.; Venanzi, L. M. *Inorg. Chem.* **1985**, *24*, 1483.
(21) Benn, R.; Brenneke, H.; Rufinska, A. *Inorg. Chem.* **1987**, *226*, 2826. Benn, R.; Brevard, C. *J. Am. Chem. Soc.* **1986**, *108*, 5622.
(22) Albinati, A.; Lehner, H.; Venanzi, L. M.; Wolfer, M. *Inorg. Chem.* **1987**, *26*, 3933.
(23) Ott, J. Dissertation No. 8000, ETH Zürich, 1986. Wolfer, M. Dissertation No. 8151, ETH Zürich, 1986. Lehner, H. Dissertation No. 7239, ETH Zürich, 1983.

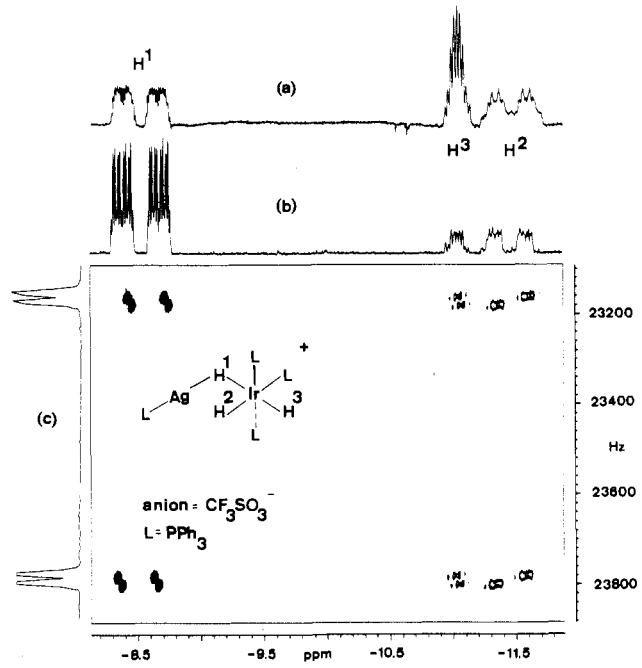

Figure 3. NMR spectra of **3**: (a) normal ^1H NMR spectrum; (b) ^1H NMR spectrum without couplings due to ^{107}Ag nuclei; (c) 2-D inverse proton-decoupled ^{109}Ag NMR spectrum.

the $J(Ag,H)$ values of 23 and 15 Hz to H^2 and H^3, respectively. These are the first established examples of silver–hydride couplings via both a bridging hydride, $^3J(Ag,H^{2\text{ or }3})$, and a metal–metal bond, $^2J(Ag,H^{2\text{ or }3})$. When these are taken together with the one-bond values, one can now more clearly define (a) when a hydride interacts strongly with Ag and when it does not, e.g., H^1 vs H^2, and (b) when relatively rapid exchange processes are present; e.g., for $[\{RhH_3(tripod)Ag\}_3]^{3+}$,[24] the observed $J(Ag,H)$ is only 44 Hz, and for $Ag\{ReH_7(PPh\text{-}i\text{-}Pr_2)_2\}_2$,[25] the $J(Ag,H)$ value is only 23 Hz. Interestingly, $^2J(P^1,H^1)$ is relatively small, ca. 33 Hz (the analogous value in **1** is 79 Hz), and we take this to imply an even larger distortion from linearity for the angle P^1–Ag–H^1, in **3**, than was observed in the structure of **1b**. A similar inverse measurement was performed on **4**, and its ^{109}Ag NMR parameters, together with other pertinent NMR data for **3** and **4**, are given in Table I and in the Experimental Section.

In the preliminary communication mention was made of the formation of small amounts of another compound which was not identified at that time. We have now established that it is $[\{(fac\text{-}IrH_3(PPh_3)_3\}_2Ag]^+$ (**5**). However, this complex is not formed when complexes **1–4** are prepared exactly as described in the Experimental Section. The chemistry and X-ray structure of compound **5** will be the subject of a later publication.

X-ray Crystal Structure of $[(PPh_3)Ag(\mu\text{-}H)IrH_2(PPh_3)_3](CF_3SO_3)\cdot 2C_6H_6$ ($3\cdot 2C_6H_6$). The structure of this compound consists of discrete cations, $CF_3SO_3^-$ anions, and clathrated benzene. An ORTEP view of the metal and donor atoms in the cation is shown in Figure 4. A list of relevant bond lengths and angles is given in Table II.

The structure of this cation is very similar to that of the corresponding gold complex. The cation consists of an octahedrally coordinated iridium atom joined to a silver atom through one, or possibly two, Ag–H–Ir bridges. It proved possible to locate the hydride ligands on Fourier difference maps by energy minimization (see the Experimental Section). These maps, however, gave ambiguous results for one of the bridging hydride ligands, H^2. Considering that in the gold compound **1b** a P^1–Au–Ir angle of 155.3 (3)° is associated with the single P^1–Au–H^1–Ir bridge and assuming that a doubly bridged arrangement would give a P^1–

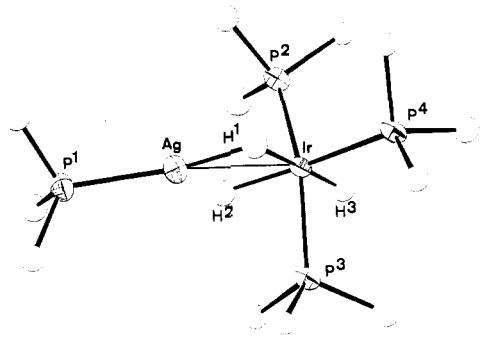

Figure 4. ORTEP drawing of the metal and donor atoms in the $[(PPh_3)Ag(\mu\text{-}H)IrH_2(PPh_3)_3]^+$ cation.

Table III. Crystallographic Data and Data Collection Parameters for the X-ray Diffraction Study of $\mathbf{1b}\cdot CH_2Cl_2$ and $\mathbf{3}\cdot 2C_6H_6$

formula	$C_{73}H_{65}AuBCl_2F_4IrP_4$	$C_{85}H_{75}AgF_3IrO_3P_4S$
fw	1613.11	1657.56
space group	$P\bar{1}$ (No. 2)	Cc (No. 9)
T	room temp	room temp
a, Å	17.482 (6)	19.461 (4)
b, Å	15.617 (5)	19.458 (5)
c, Å	13.218 (5)	20.054 (4)
α, deg	90.97 (4)[a]	
β, deg	71.38 (3)	96.16 (2)
γ, deg	103.89 (5)	
V, Å^3	3312.9 (4)	7550.3 (4)
Z	2	4
ρ_{calcd}, g cm^{-3}	1.617	1.458
λ,[b] Å	0.71069	0.71069
μ, cm^{-1}	43.60	21.75
transmission coeff	0.75–0.98	0.93–0.99
R[c]	0.054	0.049
R_w[c]	0.066	0.054

[a] Erroneously given as 91.9 (2)° in ref 5. [b] Graphite-monochromated Mo Kᾱ. [c] For the observed reflections: $R = \sum(|F_o| - 1/k|F_c|)/\sum|F_o|$; $R_w = [\sum w(|F_o| - 1/k|F_c|)^2/\sum w|F_o|^2]^{1/2}$.

Ag–Ir angle approaching 180°, the P^1–Ag–Ir angle of 160.1 (2)° suggests that the structure of the silver compound may be more appropriately described as having a single bridge.

There are relatively few known structures containing Ag–M bonds. Cotton et al. find 2.637 (1) Å for the unsupported Ag–Pt bond length in $(C_6F_5)_3(SC_4H_8)PtAg(PPh_3)$,[26] and Uson et al. report values of 2.726 (2) and 2.702 (2) Å for the Au–Ag bonds in $\{AuAg(C_6F_5)_2(SC_4H_8)\}_n$ and $\{AuAg(C_6F_5)_2(C_6H_6)_n\}$, respectively.[27] The Pt–Ag separations of 2.772 (3) and 2.796 (2) Å for $[NBu_4]_2[Pt_2Ag_2Cl_4(C_6F_5)_4]$ and $[NBu_4]_2[PtAgCl_2(C_6F_5)_2PPh_3]$, respectively, reported by Uson et al.,[28] are slightly longer. These authors assign the 2.772 (3) Å bond length to "a platinum–silver bond, perhaps one of considerable strength". The mean Re–Ag distance in $Ag\{ReH_7(PPh\text{-}i\text{-}Pr_2)_2\}_2$,[25] 2.873 (2) Å, is also taken as indicative of a metal–metal interaction. Consequently, we feel justified in considering our Ag–Ir separation of 2.758 (2) Å as indicative of some metal–metal bonding. As the ^{109}Ag NMR and X-ray data suggest that only H^1 is bridging, one might expect the terminal hydride H^2 to exert a substantial structural trans influence, and this is indeed the case. Ir–P^4 (2.362 (5) Å) is longer than either Ir–P^2 (2.328 (5) Å) or Ir–P^3 (2.291 (5) Å), thereby supporting the assignment of only one hydride ligand as bridging. We note that for **1b** Ir–P^4, at 2.397 (4) Å, is also significantly longer than either Ir–P^2 or Ir–P^3 and take this as further support for its proposed structure.

The only other significant difference between the two structures is the length of the P–Ag bond, which is longer than the P–Au

(24) Bachechi, F.; Ott, J.; Venanzi, L. M. *J. Am. Chem. Soc.* **1985**, *107*, 1760.
(25) For comparison see e.g.: Connelly, N. G.; Howard, J. A. K.; Spencer, J. L.; Woodley, P. K. *J. Chem. Soc., Dalton Trans.* **1984**, 2003.
(26) Cotton, F. A.; Falvello, L. R.; Uson, R.; Fornies, J.; Tomas, M.; Casas, J. M.; Ara, I. *Inorg. Chem.* **1987**, *26*, 1366.
(27) Uson, R.; Laguna, A.; Laguna, M.; Manzano, B. R.; Jones, P. G.; Sheldrick, G. M. *J. Chem. Soc., Dalton Trans.* **1984**, 285.
(28) Uson, R.; Fornies, J.; Menjon, B.; Cotton, F. A.; Falvello, L. R.; Tomas, M. *Inorg. Chem.* **1985**, *24*, 4651.

Table IV. Final Positional and Thermal Factors for the Cation $[(PPh_3)Au(\mu\text{-}H)IrH_2(PPh_3)_3]^+$ (B_{eq} for Au, Ir, and P Atoms; B_{iso} for the Others)

	x/a	y/b	z/c	$B_{eq,iso}$, Å^2		x/a	y/b	z/c	$B_{eq,iso}$, Å^2
Au	0.22832 (5)	0.38142 (5)	0.11811 (6)	3.24	C^{234}	0.027 (1)	−0.028 (1)	0.355 (2)	6.1 (5)
Ir	0.24708 (4)	0.23893 (5)	−0.00437 (6)	2.23	C^{235}	0.100 (2)	−0.017 (2)	0.374 (2)	7.2 (7)
P^1	0.1541 (3)	0.4521 (4)	0.2553 (4)	3.4	C^{236}	0.179 (1)	0.039 (1)	0.299 (2)	5.6 (5)
P^2	0.2700 (3)	0.1478 (3)	0.1154 (4)	3.0	C^{311}	0.051 (1)	0.216 (1)	−0.013 (1)	3.8 (4)
P^3	0.1597 (3)	0.2735 (3)	−0.0896 (4)	2.9	C^{312}	0.013 (2)	0.139 (2)	−0.043 (3)	5.1 (9)
P^4	0.3777 (3)	0.2626 (3)	−0.1461 (4)	2.6	C^{313}	−0.068 (3)	0.090 (3)	0.020 (3)	6.2 (9)
C^{111}	0.057 (1)	0.372 (1)	0.329 (2)	3.8 (4)	C^{314}	−0.111 (2)	0.126 (3)	0.111 (3)	6.6 (9)
C^{112}	0.067 (2)	0.292 (3)	0.360 (3)	5.8 (9)	C^{315}	−0.068 (2)	0.207 (2)	0.140 (3)	5.9 (9)
C^{113}	−0.004 (2)	0.223 (3)	0.408 (3)	6.6 (9)	C^{316}	0.013 (2)	0.252 (2)	−0.077 (3)	4.7 (8)
C^{114}	−0.081 (3)	0.240 (3)	0.434 (3)	7.2 (9)	C^{321}	0.153 (2)	0.386 (2)	−0.107 (2)	3.4 (7)
C^{115}	−0.091 (3)	0.321 (3)	0.401 (4)	9.3 (9)	C^{322}	0.230 (2)	0.454 (2)	−0.136 (3)	4.8 (8)
C^{116}	−0.017 (2)	0.394 (3)	0.353 (3)	5.7 (9)	C^{323}	0.230 (2)	0.543 (2)	−0.163 (3)	4.5 (8)
C^{121}	0.131 (1)	0.550 (1)	0.226 (1)	4.3 (5)	C^{324}	0.082 (2)	0.495 (2)	−0.129 (3)	5.8 (9)
C^{122}	0.151 (2)	0.582 (2)	0.117 (3)	4.7 (8)	C^{325}	0.077 (2)	0.404 (2)	−0.102 (3)	4.4 (8)
C^{123}	0.138 (2)	0.667 (3)	0.091 (3)	6.7 (9)	C^{326}	0.156 (2)	0.562 (2)	−0.157 (3)	5.2 (8)
C^{124}	0.101 (2)	0.713 (3)	0.171 (3)	6.1 (9)	C^{331}	0.172 (2)	0.234 (2)	−0.223 (2)	3.4 (7)
C^{125}	0.080 (3)	0.689 (3)	0.281 (3)	7.3 (9)	C^{332}	0.194 (2)	0.153 (2)	−0.249 (3)	4.5 (8)
C^{126}	0.096 (3)	0.604 (3)	0.305 (3)	6.9 (9)	C^{333}	0.204 (2)	0.126 (2)	−0.349 (3)	4.6 (8)
C^{131}	0.206 (1)	0.486 (1)	0.354 (2)	3.8 (4)	C^{334}	0.194 (2)	0.175 (2)	−0.428 (3)	6.0 (9)
C^{132}	0.292 (1)	0.529 (2)	0.315 (2)	7.2 (6)	C^{335}	0.170 (2)	0.254 (2)	−0.405 (3)	6.2 (9)
C^{133}	0.333 (1)	0.560 (1)	0.391 (2)	6.7 (6)	C^{336}	0.155 (2)	0.285 (2)	−0.302 (3)	5.1 (8)
C^{134}	0.287 (1)	0.556 (2)	0.496 (2)	6.6 (6)	C^{411}	0.468 (1)	0.286 (1)	−0.098 (1)	2.8 (4)
C^{135}	0.213 (1)	0.515 (2)	0.533 (2)	7.0 (6)	C^{412}	0.539 (2)	0.259 (2)	−0.153 (3)	4.6 (8)
C^{136}	0.163 (1)	0.471 (2)	0.460 (2)	6.1 (6)	C^{413}	0.611 (1)	0.277 (1)	−0.114 (2)	6.4 (6)
C^{211}	0.331 (1)	0.193 (1)	0.207 (1)	3.2 (4)	C^{414}	0.605 (1)	0.319 (2)	−0.021 (2)	6.9 (7)
C^{212}	0.315 (1)	0.266 (1)	0.258 (1)	3.9 (4)	C^{415}	0.534 (1)	0.348 (2)	0.029 (2)	7.1 (6)
C^{213}	0.352 (1)	0.301 (1)	0.334 (2)	5.1 (5)	C^{416}	0.466 (1)	0.331 (1)	−0.006 (2)	5.1 (5)
C^{214}	0.406 (1)	0.260 (1)	0.357 (2)	4.9 (5)	C^{421}	0.401 (1)	0.362 (1)	−0.235 (1)	3.1 (4)
C^{215}	0.422 (1)	0.186 (1)	0.310 (2)	5.7 (5)	C^{422}	0.371 (1)	0.355 (2)	−0.322 (1)	3.6 (4)
C^{216}	0.385 (2)	0.150 (2)	0.228 (3)	4.8 (8)	C^{423}	0.387 (1)	0.430 (1)	−0.388 (2)	4.1 (4)
C^{221}	0.316 (2)	0.060 (2)	0.056 (3)	4.0 (8)	C^{424}	0.431 (1)	0.510 (1)	−0.364 (2)	4.9 (5)
C^{222}	0.405 (1)	0.077 (1)	−0.001 (2)	4.1 (4)	C^{425}	0.459 (1)	0.520 (1)	−0.280 (2)	4.3 (5)
C^{223}	0.435 (1)	0.013 (1)	−0.062 (2)	4.8 (5)	C^{426}	0.433 (1)	0.444 (1)	−0.212 (2)	4.2 (5)
C^{224}	0.385 (2)	−0.071 (2)	−0.063 (2)	6.7 (7)	C^{431}	0.397 (1)	0.180 (1)	−0.244 (2)	3.4 (4)
C^{225}	0.297 (1)	−0.092 (2)	−0.009 (2)	5.3 (6)	C^{432}	0.457 (2)	0.202 (2)	−0.347 (3)	4.0 (7)
C^{226}	0.264 (2)	−0.022 (2)	0.052 (3)	5.1 (8)	C^{433}	0.468 (2)	0.136 (2)	−0.418 (3)	5.5 (9)
C^{231}	0.171 (1)	0.083 (1)	0.210 (1)	3.6 (4)	C^{434}	0.423 (2)	0.049 (2)	−0.386 (3)	5.5 (8)
C^{232}	0.095 (1)	0.076 (1)	0.196 (2)	4.3 (5)	C^{435}	0.361 (2)	0.026 (2)	−0.284 (2)	3.4 (7)
C^{233}	0.021 (1)	0.017 (1)	0.267 (2)	5.3 (5)	C^{436}	0.350 (2)	0.091 (2)	−0.215 (2)	3.5 (7)

bond (2.384 (6) and 2.265 (5) Å, respectively). Such differences have been observed previously.[29]

To our knowledge the above structural data provide, for the first time, a direct comparison between fully analogous complexes of silver(I) and gold(I). These show that in situations where M–M′ bonding interactions are present these two coinage metals behave very similarly.

Experimental Section

All reactions were performed in Schlenk-type flasks under purified nitrogen. Solvents were dried prior to use and distilled under nitrogen. Infrared spectra in the region 4000–400 cm^{-1} were recorded on a Beckman IR 4250 spectrophotometer as KBr pellets. The ^{1}H and ^{31}P{^{1}H} NMR spectra were recorded at 250.13 (or 200) and 101.26 MHz, respectively, on FT Bruker 250 and 200 instruments. ^{1}H and ^{31}P chemical shifts are given relative to external $(CH_3)_4Si$ and H_3PO_4, respectively. A positive sign denotes a shift downfield of the reference. ^{109}Ag spectra were measured with a Bruker AM-400 spectrometer using standard pulse sequences.[30]

A. Syntheses. *mer*-$IrH_3(PPh_3)_3$,[31] $AuCl(PPh_3)$,[32] and $AuCl(PEt_3)$[33] were prepared according to literature methods. $AgCF_3SO_3$ and $AgBF_4$ were obtained from Fluka AG and from the Aldrich Chemical Co., respectively, and used without further purification.

$[(PPh_3)Au(\mu\text{-}H)IrH_2(PPh_3)_3](CF_3SO_3)$ (1a). A solution of $AgCF_3SO_3$ (0.139 g, 0.54 mmol) in 10 mL of THF was added to a solution of $AuCl(PPh_3)$ (0.267 g, 0.54 mmol) in 10 mL of THF. The reaction mixture was stirred for 15 min and filtered through Celite, and the filtrate was reacted with a suspension of *mer*-$IrH_3(PPh_3)_3$ (0.530 g, 0.54 mmol) in 20 mL of THF. After it was stirred for 0.25 h, the clear solution was evaporated to dryness. The product was then recrystallized from CH_2Cl_2–pentane, affording colorless crystals of **1a** (0.770 g, 90%). Anal. Calcd for $C_{73}H_{63}AuF_3IrO_3P_4S$ (M_r = 1590.45): C, 55.13; H, 3.99. Found: C, 55.10; H, 3.99. IR (KBr): 2080 mw [ν(Ir–H_{term})] cm^{-1}.

$[(PPh_3)Au(\mu\text{-}H)IrH_2(PPh_3)_3](BF_4)$ (1b) was prepared similarly by reacting *mer*-$IrH_3(PPh_3)_3$ with $AuCl(PPh_3)$ and $AgBF_4$. Recrystallization from CH_2Cl_2–heptane afforded white crystals of $[(PPh_3)Au(\mu\text{-}H)IrH_2(PPh_3)_3](BF_4)\cdot CH_2Cl_2$ (**1b**·CH_2Cl_2) in 29% yield, suitable for X-ray diffraction. Anal. Calcd for $C_{72}H_{63}AuBF_4IrP\cdot CH_2Cl_2$ (M_r = 1613.11): C, 54.35; H, 4.06. Found: C, 54.20; H, 3.89.

$[(PEt_3)Au(\mu\text{-}H)IrH_2(PPh_3)_3](CF_3SO_3)$ (2). $AuCl(PEt_3)$ (0.021 g, 0.06 mmol) and $AgCF_3SO_3$ (0.016 g, 0.06 mmol) were reacted in 3 mL of THF. After it was stirred for 5 min, the mixture was carefully filtered through Celite into a THF (3 mL) suspension of *mer*-$IrH_3(PPh_3)_3$ (0.059 g, 0.06 mmol). Reaction occurred immediately, and after filtration through Celite, the solvent was removed under reduced pressure, affording a yellow oil. The product was then purified by dissolving it in CH_2Cl_2, treating the solution with activated charcoal, and, after filtration, removing the solvent under vacuum. Recrystallization from CH_2Cl_2–Et_2O afforded white crystals of **2** (0.057 g, 65%). Anal. Calcd for $C_{61}H_{63}AuF_3IrO_3P_4S$ (M_r = 1446.32): C, 50.66; H, 4.39. Found: C, 50.80; H, 4.52. IR (KBr): 2140 w and 2080 m [ν(Ir–H_{term})] cm^{-1}. ^{1}H NMR (CD_2Cl_2, room temperature): δ 6.90–7.35 (45 H, aromatic H), 1.47 (dq, 6 H, CH_2, ^3J(H,H) = 7.3 Hz, ^2J(P^1,H) = 7.0 Hz), 0.73 (dt, 9 H, CH_3, ^3J(H,H) = 7.3 Hz, ^3J(P^1,H) = 19.5 Hz).

$[(PPh_3)Ag(\mu\text{-}H)IrH_2(PPh_3)_3](CF_3SO_3)$ (3). A solution of PPh_3 (0.037 g, 0.14 mmol) and $AgCF_3SO_3$ (0.036 g, 0.14 mmol) in THF (3 mL) was added slowly to a stirred suspension of *mer*-$IrH_3(PPh_3)_3$ (0.317 g, 0.14 mmol) in THF (3 mL). The resulting pale yellow solution was heated to reflux for 5 min. The solvent was then removed under reduced pressure, affording a yellow oil. The oil was redissolved in CH_2Cl_2 (5

(29) Borrow, M.; Bürgi, H.-B.; Johnson, D. K.; Venanzi, L. M. *J. Am. Chem. Soc.* **1976**, *98*, 2356. Alyea, E. C.; Ferguson, G.; Somogyvari, A. *Inorg. Chem.* **1982**, *21*, 1369. Socol, S. M.; Jacobson, R. A.; Verkade, J. G. *Inorg. Chem.* **1984**, *23*, 88. Guy, J. J.; Jones, P. G.; Sheldrick, G. M. *Acta Crystallogr.* **1976**, *B32*, 1937. Muir, J. A.; Muir, M. M.; Lorca, E. *Acta Crystallogr.* **1980**, *B36*, 931.
(30) Bax, A. *J. Magn. Reson.* **1983**, *55*, 301. Shaka, A. J.; Keeler, J.; Freeman, R. *J. Magn. Reson.* **1983**, *55*, 313.
(31) Chatt, J.; Coffey, R. S.; Shaw, B. L. *J. Chem. Soc.* **1965**, 7391.
(32) Levi-Malvano, A. *Atti R. Accad. Naz. Lincei, Mem. Cl. Sci. Fis., Mat. Nat.* **1908**, *17*, 857.
(33) Mann, F. G.; Wells, A. F.; Purdie, D. *J. Chem. Soc.* **1937**, 1828.

Table V. Final Positional and Thermal Factors for $[(PPh_3)Ag(\mu\text{-}H)IrH_2(PPh_3)_3](CF_3SO_3)\cdot 2C_6H_6$ (B_{eq} for Ag, Ir, and P Atoms, B_{iso} for the Others)[a]

	x/a	y/b	z/c	$B_{eq,iso}$, Å^3		x/a	y/b	z/c	$B_{eq,iso}$, Å^3
Ir	0.508	0.28603 (5)	0.085	2.89 (1)	C^{232}	0.709 (2)	0.269 (2)	0.275 (2)	6.9 (8)
Ag	0.4936 (1)	0.2070 (1)	0.1967 (1)	4.87 (5)	C^{233}	0.434 (2)	0.527 (2)	0.205 (2)	8 (1)
P^1	0.4478 (4)	0.1643 (4)	0.2942 (4)	4.2 (2)	C^{241}	0.683 (2)	0.539 (2)	0.054 (2)	7.5 (9)
P^2	0.5579 (3)	0.3704 (4)	0.1537 (4)	4.0 (2)	C^{242}	0.715 (2)	0.309 (2)	0.333 (2)	8.0 (9)
P^3	0.4141 (3)	0.2299 (3)	0.0270 (4)	3.6 (2)	C^{243}	0.389 (2)	0.494 (2)	0.243 (2)	9 (1)
P^4	0.5923 (3)	0.2722 (3)	0.0090 (4)	3.6 (2)	C^{251}	0.707 (2)	0.510 (2)	0.118 (2)	7.9 (9)
C^{11}	0.382 (1)	0.221 (1)	0.325 (1)	4.6 (6)	C^{252}	0.673 (2)	0.365 (2)	0.343 (2)	7.5 (9)
C^{12}	0.332 (1)	0.244 (1)	0.274 (1)	5.0 (6)	C^{253}	0.395 (2)	0.427 (2)	0.259 (2)	11 (1)
C^{13}	0.281 (2)	0.289 (2)	0.299 (2)	8.5 (9)	C^{261}	0.669 (2)	0.464 (2)	0.144 (2)	6.3 (8)
C^{14}	0.277 (2)	0.302 (2)	0.364 (2)	6.3 (8)	C^{411}	0.685 (1)	0.270 (1)	0.052 (1)	3.2 (5)
C^{15}	0.328 (2)	0.277 (2)	0.409 (2)	8.6 (9)	C^{412}	0.588 (1)	0.191 (1)	−0.038 (1)	3.6 (5)
C^{16}	0.381 (2)	0.238 (2)	0.391 (2)	6.7 (8)	C^{413}	0.596 (1)	0.334 (1)	−0.057 (1)	4.1 (6)
C^{21}	0.514 (1)	0.151 (1)	0.362 (1)	4.4 (6)	C^{421}	0.720 (2)	0.334 (2)	0.060 (2)	6.2 (8)
C^{22}	0.499 (1)	0.111 (1)	0.420 (1)	5.4 (7)	C^{422}	0.597 (1)	0.186 (1)	−0.107 (1)	5.1 (7)
C^{23}	0.550 (2)	0.109 (2)	0.472 (2)	6.4 (8)	C^{423}	0.534 (1)	0.369 (1)	−0.083 (1)	3.6 (5)
C^{24}	0.612 (2)	0.134 (2)	0.472 (2)	8 (1)	C^{431}	0.787 (2)	0.331 (2)	0.097 (2)	7.0 (8)
C^{25}	0.630 (2)	0.175 (2)	0.425 (2)	11 (1)	C^{432}	0.590 (1)	0.127 (2)	−0.141 (1)	5.5 (7)
C^{26}	0.574 (2)	0.191 (2)	0.368 (2)	7.8 (9)	C^{433}	0.537 (2)	0.415 (2)	−0.135 (2)	6.1 (7)
C^{31}	0.401 (1)	0.081 (1)	0.282 (1)	3.9 (6)	C^{441}	0.814 (1)	0.266 (1)	0.119 (1)	5.8 (7)
C^{32}	0.336 (1)	0.071 (2)	0.298 (2)	6.2 (7)	C^{442}	0.578 (2)	0.069 (2)	−0.107 (2)	7.0 (8)
C^{262}	0.616 (2)	0.380 (2)	0.288 (2)	11 (1)	C^{443}	0.596 (2)	0.425 (2)	−0.167 (2)	6.2 (7)
C^{263}	0.446 (2)	0.386 (2)	0.232 (2)	10 (1)	C^{451}	0.782 (2)	0.207 (2)	0.108 (2)	7.1 (8)
C^{311}	0.397 (1)	0.255 (1)	−0.061 (1)	4.8 (6)	C^{452}	0.567 (2)	0.071 (2)	−0.038 (2)	7.2 (9)
C^{312}	0.335 (1)	0.254 (1)	0.064 (1)	3.6 (5)	C^{453}	0.657 (2)	0.390 (2)	−0.143 (2)	6.3 (8)
C^{313}	0.405 (1)	0.136 (1)	0.024 (1)	3.1 (5)	C^{461}	0.713 (1)	0.205 (1)	0.073 (1)	4.9 (6)
C^{321}	0.428 (1)	0.218 (2)	−0.110 (1)	5.5 (6)	C^{462}	0.573 (1)	0.131 (1)	−0.004 (1)	4.7 (6)
C^{322}	0.283 (2)	0.204 (2)	0.067 (2)	7.2 (8)	C^{463}	0.661 (2)	0.347 (2)	−0.087 (2)	6.2 (8)
C^{323}	0.438 (1)	0.095 (1)	0.073 (1)	3.9 (6)	S	0.1206 (6)	0.5018 (6)	0.6736 (6)	10.4 (3)
C^{331}	0.417 (1)	0.246 (2)	−0.175 (1)	5.7 (7)	CF	0.170 (2)	0.444 (2)	0.732 (2)	13 (1)
C^{332}	0.224 (2)	0.229 (2)	0.101 (2)	8 (1)	F^1	0.225 (1)	0.428 (1)	0.712 (1)	11.6 (6)
C^{333}	0.427 (1)	0.024 (1)	0.076 (2)	5.4 (7)	F^2	0.212 (1)	0.525 (1)	0.745 (1)	15.4 (7)
C^{341}	0.378 (2)	0.303 (1)	−0.194 (2)	6.0 (7)	F^3	0.156 (1)	0.452 (1)	0.786 (1)	11.6 (6)
C^{342}	0.215 (1)	0.293 (2)	0.116 (2)	6.3 (7)	O^1	0.073 (1)	0.542 (1)	0.705 (1)	8.7 (6)
C^{343}	0.385 (2)	−0.005 (2)	0.025 (2)	9 (1)	O^2	0.087 (1)	0.421 (1)	0.667 (1)	12.2 (7)
C^{351}	0.348 (2)	0.338 (2)	−0.144 (2)	7.3 (8)	O^3	0.145 (1)	0.521 (1)	0.614 (1)	10.8 (7)
C^{352}	0.263 (2)	0.339 (2)	0.111 (2)	7.3 (9)	C^{B11}	0.497 (3)	0.265 (2)	0.574 (3)	13 (1)
C^{353}	0.351 (2)	0.033 (2)	−0.030 (2)	6.1 (7)	C^{B12}	0.522 (2)	0.327 (2)	0.600 (2)	11 (1)
C^{361}	0.357 (1)	0.314 (1)	−0.078 (1)	4.6 (6)	C^{B13}	0.550 (2)	0.326 (3)	0.664 (2)	12 (1)
C^{362}	0.325 (1)	0.322 (1)	0.082 (1)	4.8 (6)	C^{B14}	0.554 (2)	0.270 (2)	0.705 (2)	11 (1)
C^{363}	0.363 (1)	0.106 (1)	−0.027 (1)	5.3 (7)	C^{B15}	0.534 (2)	0.213 (2)	0.677 (2)	10 (1)
C^{33}	0.311 (2)	0.006 (2)	0.286 (2)	6.6 (8)	C^{B16}	0.507 (2)	0.206 (2)	0.616 (2)	10 (1)
C^{34}	0.345 (2)	−0.046 (2)	0.266 (2)	7.0 (8)	C^{B21}	0.373 (2)	0.479 (2)	0.442 (2)	12 (1)
C^{35}	0.412 (2)	−0.037 (2)	0.254 (2)	6.4 (7)	C^{B22}	0.386 (2)	0.485 (2)	0.506 (2)	11 (1)
C^{36}	0.443 (1)	0.028 (1)	0.263 (1)	5.4 (7)	C^{B23}	0.325 (3)	0.465 (3)	0.555 (3)	17 (2)
C^{211}	0.607 (1)	0.437 (1)	0.114 (1)	3.2 (5)	C^{B24}	0.263 (2)	0.491 (2)	0.512 (2)	11 (1)
C^{212}	0.618 (1)	0.345 (1)	0.226 (1)	4.5 (6)	C^{B25}	0.252 (2)	0.493 (2)	0.444 (2)	11 (1)
C^{213}	0.491 (1)	0.423 (2)	0.191 (1)	5.5 (7)	C^{B26}	0.302 (2)	0.480 (2)	0.414 (2)	11 (1)
C^{221}	0.580 (1)	0.463 (1)	0.055 (1)	5.1 (7)	H^1	0.539 (8)	0.236 (9)	0.127 (8)	5 (1)
C^{222}	0.660 (1)	0.288 (2)	0.221 (1)	5.1 (6)	H^2	0.453 (8)	0.287 (9)	0.146 (8)	−4 (1)
C^{223}	0.486 (2)	0.493 (2)	0.178 (2)	7.2 (9)	H^3	0.477 (8)	0.354 (9)	0.024 (9)	4 (1)
C^{231}	0.616 (2)	0.516 (2)	0.020 (2)	7.6 (9)					

[a] Anisotropically refined atoms are given in the form of the isotropic equivalent thermal parameter defined as $^4/_3[a^2B_{11} + b^2B_{22} + c^2B_{33} + ab(\cos\gamma)B_{12} + ac(\cos\beta)B_{13} + bc(\cos\alpha)B_{23}]$. Atoms labeled C^{B11}–C^{B26} correspond to those of the two C_6H_6 molecules.

mL), and after addition of activated charcoal the mixture was stirred for 0.5 h. After filtration, the solution was concentrated to ca. 3 mL. Hexane was added, and **3** precipitated as a white powder (0.170 g, 81%). Anal. Calcd for $C_{73}H_{63}AgF_3IrO_3P_4S$ (M_r = 1501.35): C, 58.40; H, 4.23. Found: C, 58.69; H, 4.17. IR (KBr): 2080 w and 2035 mw [ν(Ir–H_{term})] cm^{-1}. ^{1}H NMR (CD_2Cl_2, 253 K): δ 6.8–7.4 (60 H, aromatic H).

$[(PEt_3)Ag(\mu\text{-}H)IrH_2(PPh_3)_3](CF_3SO_3)$ (4). The reaction was performed with 0.026 g (0.10 mmol) of $AgCF_3SO_3$, 0.012 g (0.10 mmol) of PEt_3, and 0.098 g (0.10 mmol) of *mer*-$IrH_3(PPh_3)_3$ by the procedure given for **3**. After treatment with activated charcoal–CH_2Cl_2, the product was recrystallized from THF–hexane (colorless crystals; 0.104 g, 77%). Anal. Calcd for $C_{61}H_{63}AgF_3IrO_3P_4S$ (M_r = 1357.22): C, 53.98; H, 4.68. Found: C, 54.20; H, 4.66. IR (KBr): 2080 w and 2050 mw [ν(Ir–H_{term})] cm^{-1}. ^{1}H NMR (CD_2Cl_2, 253 K): δ 6.90–7.32 (45 H, aromatic H), 1.31 (q, 6 H, CH_2, ^3J(H,H) = 7.4 Hz, ^2J(P,H) unresolved coupling constant), 0.70 (dt, 9 H, CH_3, ^3J(H,H) = 7.4 Hz, ^3J(P,H) = 16 Hz).

B. X-ray Measurements. Crystal Structure of 1b-CH_2Cl_2. These crystals are unstable in air. A prismatic crystal was sealed in a capillary with some mother liquor to avoid decay. The determination of the lattice parameters and of the space group and data collection were carried out on a Philips PW 1100 four-circle diffractometer. The cell parameters were obtained by a least-squares fit of the 2θ values of 20 high-angle reflections ($16.0 \leq 2\theta \leq 28.0$) The crystallographic data and data collection parameters are listed in Tables III and S1 (supplementary material).

Three standard reflections $\bar{2}\bar{1}2$, $\bar{2}42$, and $2\bar{4}\bar{2}$, were measured every 2 h to check the stability and orientation of the crystal. No significant variations in the diffracted intensities were detected during the data collection. Data were corrected for Lorentz and polarization factors,[34] and an empirical absorption correction using azimuthal (ψ) scans of two reflections at high χ angle was applied; transmission factors were in the range 0.75–0.98. The standard deviations on intensities were calculated in terms of statistics alone, and reflections having $I_{net} \geq 3\sigma(I)$ were considered as observed and used for the solution and refinement of the structure.

The structure was solved by standard Patterson and Fourier methods and refined by block-diagonal least squares with a Cruickshank weighting

(34) Arndt, U. V.; Willis, B. T. M. *Single Crystal Diffractometry*; Cambridge University Press: Cambridge, England, 1966; p 286.

scheme;[35] the function minimized was $\sum w(|F_o| - 1/k|F_c|)^2$. Anisotropic temperature factors were used for the Au, Ir, and P atoms while isotropic factors were used for the remaining atoms. Scattering factors were taken from the literature,[36] and the contribution of the real part of the anomalous dispersion was taken into account for Au, Ir, and P atoms by using tabulated values.[36] No extinction correction was deemed necessary.

Upon convergence (no shifts greater than 0.5σ) a Fourier difference map revealed a clathrated CH_2Cl_2 molecule. Due to its disorder a refinement of the positional and thermal parameters failed to converge, giving an unrealistic geometry: therefore, the contribution of the atoms (using positions from the Fourier map) was taken into account but not refined. It proved impossible to locate the bridging and terminal hydrides from Fourier difference maps calculated with various cutoff limits (down to $(\sin\theta)/\lambda = 0.3$ Å^{-1});[37] their positions were located by using the program HYDEX,[38] which minimizes the nonbonded interaction energies between the hydrides and the other ligands (the starting M–H distances for bridging and terminal hydrides were assumed to be 1.80 and 1.70 Å, respectively). Four potential energy minima were found, the lowest three being consistent with the expected positions of the hydride ligands. An attempt to refine them failed to give acceptable bond lengths and thermal factors. The final atomic coordinates are given in Table IV.

Crystal Structure of 3·2C$_6$H$_6$. Colorless crystals were obtained by slow evaporation of the concentrated CD_2Cl_2 solution used for the ^{109}Ag NMR determination.[39] A prismatic crystal was chosen and mounted on a glass fiber at a random orientation. The determination of the lattice parameters and of the space group and data collection were carried out on a Nonius CAD 4 diffractometer. Systematic absences were consistent with space group Cc or $C2/c$. The noncentrosymmetric group was chosen for the structure solution and refinement on the basis of the results of a statistical $N(z)$ test[40] and later confirmed by the successful refinement. The cell parameters were obtained by a least-squares fit of the 2θ values of 25 high-angle reflections ($21.0 \leq 2\theta \leq 28.0$). The crystallographic data and data collection parameters are listed in Tables III and S1 (supplementary material).

Three standard reflections (10,0,0; −10,0,0; −7,−1,7) were measured every 1 h to check the stability of the crystal. No significant variations in the diffracted intensities were detected during the data collection. The orientation of the crystal was monitored by measuring three standards every 300 reflections. Data were corrected for Lorentz and polarization factors,[40] and an empirical absorption correction using azimuthal (ψ) scans of three reflections at high χ angle (87.0–88.6°) was applied by using the SDP programs. The standard deviations on intensities were calculated in terms of statistics alone. The standard deviations on F_o^2 were calculated according to $\sigma(F^2) = [(\sigma^2(I)) + (pI)^2]^{1/2}$ ($p = 0.045$). $F_o = 0.0$ was given to the reflections having negative net intensities.

The structure was solved by using direct as well as Patterson and Fourier methods and refined by full-matrix least squares. The function minimized was $\sum w(|F_o| - 1/k|F_c|])^2$ with $w = [\sigma(F_o)]^{-2}$. Anisotropic temperature factors were used for the Ag, Ir, and P atoms while isotropic factors were used for the remaining atoms. Scattering factors were taken from the literature,[36] and the contribution of the real and imaginary parts of the anomalous dispersion was taken into account.[36] No extinction correction was deemed necessary. All calculations were carried out by using the programs of the SDP package.[40]

In the last stages of the refinement two clathrated benzene molecules were found and successfully refined.

The structure of **3** shows a certain amount of disorder, as can be judged from the values of the thermal parameters for some atoms and the high esd's associated with the phenyl carbons. In particular, it did not prove possible to obtain an acceptable model for the highly disordered $CF_3SO_3^-$ groups. Therefore, upon convergence of the cation refinement (no shifts $>0.1\sigma$), the strongest peaks in the Fourier difference map, giving an approximate geometry for the anion, were retained and their thermal factors refined.

The contribution of the hydrogen atoms of the phenyl groups in their calculated positions (C–H = 0.95 Å, $B = 8.0$ Å^2) was taken into account but not refined.

In this complex it proved possible to locate the hydride ligands from Fourier maps. Upon convergence, Fourier differences were calculated by using both all data and a limited set ($(\sin\theta)/\lambda = 0.3$ Å^{-1}). Peaks were found near the position consistent with the presence of *mer*-$IrH_3(PPh_3)_3$. Three cycles of full-matrix refinement of this set of coordinates gave acceptable convergence (although with the expected high esd's) for the bridging (H^1) and terminal (H^3) hydrides (see Figure 4) but not for H^2 ($B = -4$ (1) Å^2; Ag–H = 2.0 (2) Å, Ir–H = 1.8 (2) Å). The relevant bond distances are, however, listed in Table II. These locations were checked by using the program HYDEX.[38] Three different energy minima were found, two of them being consistent with an Ag–H–Ir bridging moiety (Ag–H = 1.89 Å, Ir–H = 1.90 Å) and one with a terminal Ir–H bond (Ir–H = 1.72 Å). It is, however, possible that the doubly bridged structure is an artifact of the minimization procedure and its insensitivity to the values of the potentials used for the heavy metals.

In conclusion neither method provides reliable information as to whether, in the solid state, the hydride ligand H^2 is bridging, semibridging, or even terminal.

The handedness of the crystal was tested by refining the two possible sets of coordinates; those giving a significantly lower R_w factor[41] (R_w = 0.054 as compared with 0.077 for the other enantiomer) are listed in Table V.

Acknowledgment. Support of this work by the Swiss National Science Foundation (P.J. and H.L.) and by NATO (Grant No. 85/068, A.A.) is gratefully acknowledged.

Registry No. **1a**, 118831-54-2; **1b**, 83527-81-5; **1b**·CH_2Cl_2, 118831-55-3; **2**, 118831-56-4; **3**, 118831-57-5; **3**·2C_6H_6, 118831-59-7; **4**, 118831-58-6; $AuCl(PPh_3)$, 14243-64-2; *mer*-$IrH_3(PPh_3)_3$, 18660-47-4; $AuCl(PEt_3)$, 15529-90-5; Ir, 7439-88-5; Ag, 7440-22-4; Au, 7440-57-5; ^{109}Ag, 14378-38-2.

Supplementary Material Available: Tables containing details of the data collection for **1b** and **3** (Table S1), atomic thermal parameters for **3** (Table S2), and an extensive list of interatomic distances and angles for **3** (Table S3), an ORTEP view of the cation of **1b** (Figure S1), an ORTEP view of the cation of **3** (Figure S2), and a numbering scheme for the cation of **3** (Figure S3) (13 pages); observed and calculated structure factors for **3** (Table S4) (15 pages). Ordering information is given on any current masthead page. Tables of thermal parameters, interatomic distances and angles, and structure factors for **1b** are obtainable as described in ref 5.

(35) Cruickshank, D. W. J. In *Computing Methods in Crystallography*; Ahmed, A., Ed.; Munksgaard: Copenhagen, 1972.
(36) *International Tables for X-Ray Crystallography*; Kynoch Press: Birmingham, England, 1974; Vol. IV.
(37) Teller, R. G.; Bau, R. *Struct. Bonding (Berlin)* **1981**, *44*, 1.
(38) Orpen, A. G. *J. Chem. Soc., Dalton Trans.* **1980**, 2509.
(39) The clathrated benzene molecules must have been formed during crystal growth, possibly by P–Ph bond cleavage as found in other PPh_3 complexes; e.g., see: Jans, J.; et al. *J. Organomet. Chem.* **1983**, *247*, C37.
(40) "Enraf-Nonius Structure Determination Package (SDP)"; Enraf-Nonius: Delft, Holland, 1980.
(41) Hamilton, W. C. *Acta Crystallogr.* **1965**, *13*, 502.